Design and Performance Tests of a Low Power DC Arcjet Thruster

By

Michio NISHIDA*, Keiji KAITA* and Ken-ichi TANAKA**

(Received June 30, 1987)

Abstract

This paper describes a quasi-one-dimensional flow model which can be used for the design of an arcjet thruster. Owing to the simplicity of the model, the performance characteristics of the thruster can be calculated easily for finding an optimum configuration suitable for various missions. In order to verify adequacy of the model, a thruster was fabricated and its performance characteristics were measured. The experimental results were compared with the calculation predicted with the model. Both are in satisfactory agreement, and it is concluded that this flow model is a useful tool for the design of the arcjet thruster.

Nomenclature

A = cross-sectional area
C_p = specific heat at constant pressure
F = thrust
I_{sp} = specific impulse
M = Mach number
P_w = input power
R = gas constant
T = temperature
a = velocity of sound
g = gravitational constant
$\dot{m}$ = mass flow rate
p = pressure
u = velocity
η_p = power conversion efficiency
γ = ratio of specific heats
ρ = density
ϕ = diameter

Subscripts

0 = stagnation
1 = inlet of discharge section
2 = outlet of discharge section
$*$ = nozzle throat
e = nozzle exit
∞ = ambient condition

* Department of Aeronautical Engineering.
** Central Research Laboratory, Mitsubishi Electric Corporation.

1. Introduction

As spacecraft becomes larger and the lifetime becomes longer, a thruster, which has a higher specific impulse than the currently used cold gas jet thruster, is indispensable to control the motion of the spacecraft. An arcjet thruster is one of the candidates for this purpose. In order to predict the performance of the arcjet thruster, the approximate method using the law of energy conservation has been extensively employed. However, this method is rough in its accuracy, so that it cannot be sufficiently put to practical use. Recently, a computational simulation of the flowfields inside an arcjet thruster has been developed by using an axisymmetric arcjet thruster model[1),2)]. This computational simulation is suitable to make the computational flow visualization from calculated data. However, it takes much time to obtain the solution. Owing to these shortcomings, it is not adequate to use this simulation method in designing the arcjet thruster, in which the design parameters such as the dimension of the thruster and the property of the propellant are often altered to find the optimum configurations. Therefore, an easily treatable method, which is applied to determine the thruster performance, such as the thrust and the specific impulse from the given design parameters, is required. A quasi-one-dimensional flow model is proposed in the present paper for this purpose. An arcjet thruster which has the same dimensional specification as this model was constructed and its performance characteristics were measured. The experimental results were compared with the calculation in order to examine the usefulness of this model.

2. Thruster Flow Model

Figure 1 shows the scheme of the arcjet thruster model. In this model, a flow inside the thruster is assumed to be quasi-one-dimensional, and a propellant gas follows the equation of state for an ideal gas. We also assume that there is no shock wave in the flowfield. The thruster model is divided into the following four sections.

1) From the stagnation chamber to the inlet of the discharge section
2) In the discharge section
3) From the outlet of the discharge section to the nozzle throat
4) From the nozzle throat to the nozzle exit

The propellant gas isentropically flows from the stagnation chamber (subscript 0) to the inlet of the discharge section (subscript 1) where the flow is still subsonic. At the discharge section, the electrical power is injected into the propellant by a DC

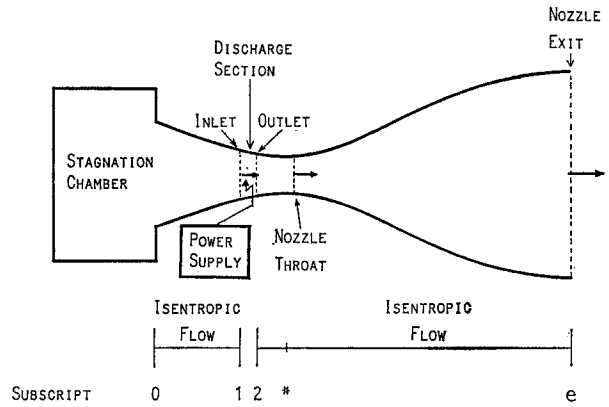

Fig. 1. Arcjet Thruster Flow Model.

arc, and the stagnation enthalpy of the propellant at the outlet of the discharge section (subscript 2) increases. For simplicity, the width of the discharge section in the flow direction is very small so that the cross-sectional areas at the inlet and the outlet are assumed to be equal. From the outlet of the discharge section to the nozzle throat (subscript*), the flow is isentropic, and the velocity of the propellant becomes equal to the velocity of sound at the nozzle throat. From the nozzle throat to the nozzle exit (subscript e), the flow isentropically expands. At the nozzle exit the propellant flow is supersonic. The flow properties such as velocity, pressure, temperature and density at each station are derived as follows:

1) From the stagnation chamber to the inlet of the discharge section

For a specified nozzle dimension, the cross-sectional areas A_1 and A_* are known, so that the Mach number at the inlet of the discharge section, M_1, is given by

$$\left(\frac{A_1}{A_*}\right)^2 = \frac{1}{M_1^2}\left[\frac{\gamma+1}{2}\left(1+\frac{\gamma-1}{2}M_1^2\right)\right]^{(\gamma+1)/(\gamma-1)}, \tag{1}$$

where γ is the ratio of specific heats. Other flow properties at the inlet are obtained from

$$\begin{aligned} &C_p T_0 = C_p T_1 + \frac{1}{2}u_1^2, \\ &u_1 = \sqrt{\gamma R T_1}\, M_1, \\ &\frac{p_1}{p_0} = \left(1+\frac{\gamma-1}{2}M_1^2\right)^{-\gamma/(\gamma-1)}, \\ &\rho_1 = \frac{p_1}{RT_1}, \end{aligned} \tag{2}$$

where C_p is the specific heat at constant pressure, T is the temperature, u is the velocity of the propellant, R is the gas constant, p is the pressure and ρ is the density. The first equation in Eq. (2) comes from the law of energy conservation, the second from the definition of the Mach number, the third from the relation of the pressure for the isentropic flow and the last from the equation of state. Solving Eq. (1) for M_1, and substituting it and given properties at the stagnation chamber into Eq. (2), we can obtain flow properties at the inlet of the discharge section.

2) In the discharge section

At the discharge section, the propellant is heated by electrical power. The stagnation temperatures before (at the inlet) and after (at the outlet) heating have the following relation,

$$\frac{T_{02}}{T_{01}} = \frac{M_2^2(1+\gamma M_1^2)^2\left(1+\frac{\gamma-1}{2}M_2^2\right)}{M_1^2(1+\gamma M_2^2)^2\left(1+\frac{\gamma-1}{2}M_1^2\right)}. \tag{3}$$

The stagnation temperature after heating is given by

$$T_{02} = T_{01}+\frac{\eta_p P_w}{A_1\rho_1 u_1 C_p}, \tag{4}$$

where P_w is the input power and η_p is the power conversion efficiency, i.e., the ratio of the energy injected to the propellant to the electrical input energy. The second term of the right-hand side denotes the heating effect. Substituting Eq. (4) into Eq. (3) gives the Mach number at the outlet of the discharge section, M_2. Other properties are obtained as follows:

$$\begin{aligned}
\frac{p_2}{p_1} &= \frac{1+\gamma M_1^2}{1+\gamma M_2^2}, \\
\frac{\rho_2}{\rho_1} &= \frac{M_1^2}{M_2^2}\left(\frac{1+\gamma M_2^2}{1+\gamma M_1^2}\right), \\
T_2 &= \frac{p_2}{R\rho_2}.
\end{aligned} \tag{5}$$

3) From the outlet of the discharge section to the nozzle throat

From the outlet of the discharge section to the nozzle throat, the propellant isentropically flows. As we assume that the Mach number at the nozzle throat is equal to unity, the relations between the properties at the outlet and the throat are given by

$$
\begin{aligned}
&C_p T_2+\frac{1}{2}u_2^2 = C_p T_*+\frac{1}{2}a_*^2 ,\\
&A_2\rho_2 u_2 = A_*\rho_* a_* ,\\
&p_* = \rho_* R T_* ,
\end{aligned}
\tag{6}
$$

where a is the speed of sound. The second equation represents the law of mass conservation.

4) From the nozzle throat to the nozzle exit

The flow from the nozzle throat to the nozzle exit is isentropic. The same equations used at the first section also hold for this section. Rewriting Eqs. (1) and (2), we obtain

$$
\left(\frac{A_e}{A_*}\right)^2 = \frac{1}{M_e^2}\left[\frac{2}{\gamma+1}\left(1+\frac{\gamma-1}{2}M_e^2\right)\right]^{(\gamma+1)/(\gamma-1)} ,
\tag{7}
$$

and

$$
\begin{aligned}
&C_p T_e+\frac{1}{2}u_e^2 = C_p T_*+\frac{1}{2}a_*^2 ,\\
&u_e = \sqrt{\gamma R T_e}\, M_e ,\\
&\frac{p_e}{p_*} = \left(1+\frac{\gamma-1}{2}M_e^2\right)^{-\gamma/(\gamma-1)} ,\\
&\rho_e = \frac{p_e}{R T_e} .
\end{aligned}
\tag{8}
$$

Solving Eq. (7) for M_e and substituting it into Eq. (8), the flow properties at the nozzle exit are determined. The thruster performance can be calculated by substituting the flow properties at the nozzle exit into the definitions described below:

$$
\begin{aligned}
&\dot{m} = A_e\rho_e u_e ,\\
&F = (p_e-p_\infty)A_e+\dot{m}u_e ,\\
&I_{sp} = \frac{F}{\dot{m}g} ,
\end{aligned}
$$

where $\dot{m}$ is the mass flow rate of the propellant, F is the thrust, I_{sp} is the specific impulse, p_∞ is the ambient pressure and g is the gravitational constant.

3. Design of a Thruster

In order to examine the usefulness of the model, an arcjet thruster was designed.

The target of the arcjet thruster in the present work is a low power (0.5–1 kw) DC arcjet thruster with a radiation cooling system. The mission of the thruster considered here is the North-South station keeping of a 1-ton class spacecraft which has the lifetime of ten years. The given specification of the thruster is tabulated in Table 1. According to this specification, a thruster was designed by using the quasi-one-dimensional model mentioned above. In Fig. 2, the relations between the design parameters and the thruster performance are shown. In the figure, a gradient of each arrow depicts the degree of effect to the thruster performance when a design parameter is increased by 10% from its nominal value while keeping other parameters constant. From this figure, the following points are summarized:

1) The nozzle throat area (A_*) significantly affects the thruster performance.
2) To increase the specific impulse, the nozzle throat area should be small and

Table 1 Given Specification of Thruster

item	specification
input power	1000 W
specific impulse	≥320 s
propellant	hydrazine (N_2H_4)
temperature	973 K
mass flow rate (nominal)	0.083 g/s

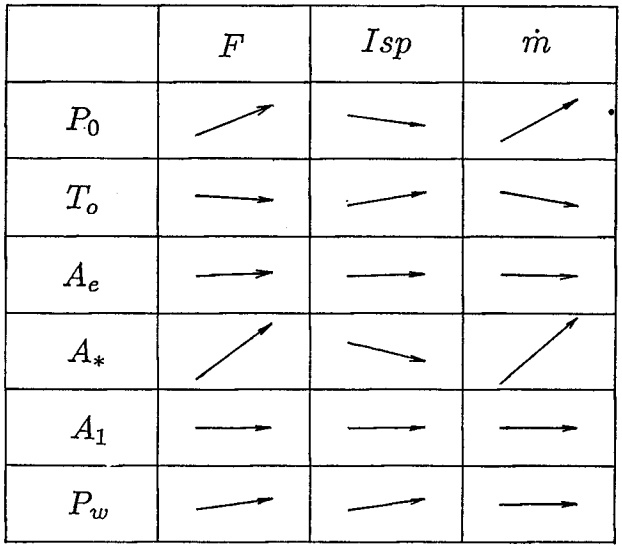

Fig. 2. Influence of the Design Parameters on Performance.

the nozzle exit area (A_e) should be large. But the large nozzle exit is less effective because it increases the weight of the thruster.

3) For the small change of the cross-sectional area at the discharge section (A_1), there is no change in the thruster performance, namely, the thruster performance is not so sensitive to the change of the cross-sectional area at the discharge section in the vicinity of the design point.

According to the results in Fig. 2, the thruster performance, which satisfies the specification given in Table 1, has been determined as follows:

$$\phi_e = 25 \text{ mm}, \quad \phi_* = 2 \text{ mm} \quad \text{and} \quad \phi_1 = 7 \text{ mm}$$

where ϕ_e, ϕ_* and ϕ_1 are the diameters of the nozzle exit, the throat and the discharge section, respectively. The value of 0.25 was used for η_p, which is empirically given. The mass flow rate-thrust, mass flow rate-specific impulse characteristics for this thruster are shown in Figs. 3(a) and 3(b), and the thruster performance at the design point is tabulated in Table 2.

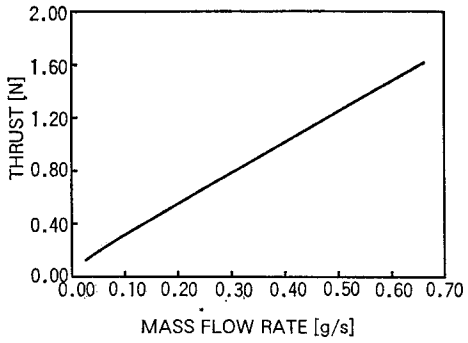

(a)

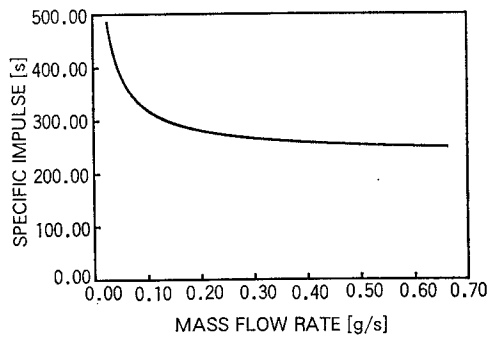

(b)

Fig. 3 (a) Mass Flow Rate—Thrust Characteristics (Hydrazine).

Fig. 3 (b) Mass Flow Rate—Specific Impulse Characteristics (Hydrazine).

Table 2 Designed Specification of Thruster

item	specification
exit diameter	25 mm
throat diameter	2 mm
discharge sec. dia.	7 mm
thrust	0.272 N
specific impulse	336 s
mass flow rate	0.083 g/s

4. Experiment

Figure 4 shows a cross-section of the thruster. The cathode and anode were made of thoriated tungsten, and an insulator was made of boron-nitride. Five holes were drilled in the anode to measure the temperature at the nozzle wall with thermoelectric couples. The pictures of the thruster and the cathode are shown in Fig. 5. The weight of the thruster is 2000 g.

The experimental block diagram is shown in Fig. 6. The thruster was mounted on a balance which was supported by a sharp wedge. The moment of the thrust about the sharp wedge was detected by a load cell. The load cell detects the moment caused by the thrust as well as the moment caused by the unnecessary force such as reaction force from power cables and a propellant supply tube. To obtain the magnitude of the thrust, the measured data should be calibrated. For this purpose another load cell set at the micrometer head was provided. By moving this head, force was exerted onto the thruster. Thus, from the outputs of the two load cells, a calibration curve was determined. The experiment was carried out in a vacuum chamber with a volume of 2700 liters, and under the conditions of mass flow rate from 0.07 g/sec to 0.42 g/sec. The ambient pressure in the chamber was kept below 0.1 torr (13.3 Pa) and the arc current was constantly kept at 80 A during the experiment. Argon was used as the propellant, because hydrazine is explosive and dangerous. The thruster in operation is shown in Fig. 7. In this figure, 20 minutes have passed since the thruster started to operate, and the temperature of of the thruster was steady. The measured temperatures at the three stations (described by 1, 3 and 5) shown in Fig. 4 were, respectively, 1190 K, 1270 K and 1270 K. The arc characteristics of the thruster are shown in Fig. 8. The arc voltage slightly decreases as the mass flow rate increases, becomes minimum at 0.083

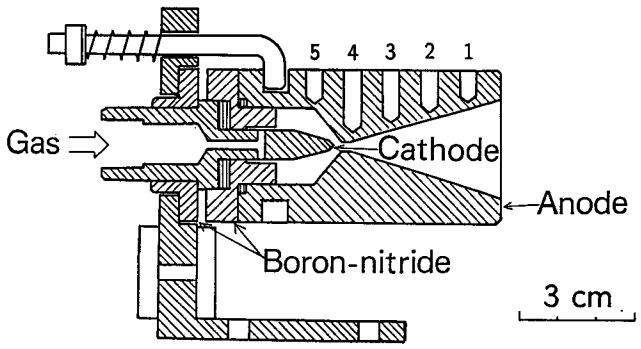

Fig. 4. Cross Section of the Thruster.

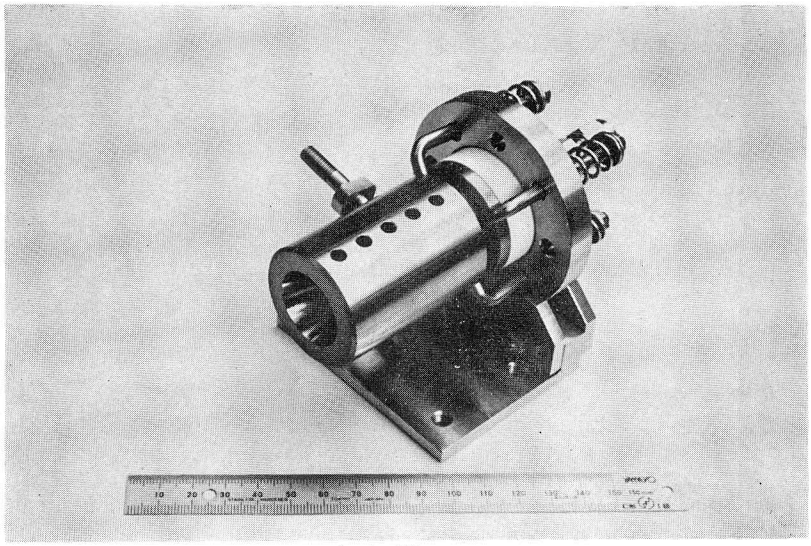

Arcjet Thruster

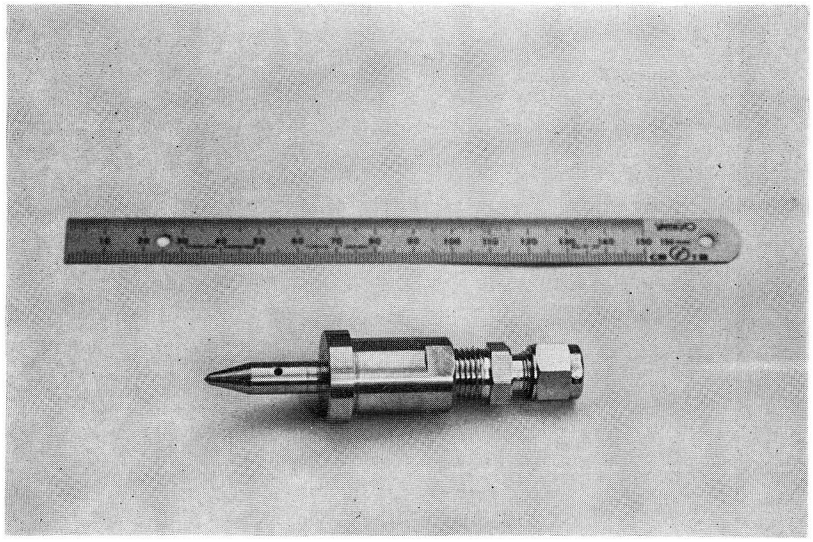

Cathode

Fig. 5. Picture of the Thruster and Cathode.

g/s and increases monotonically as the mass flow rate increases. This characteristic is different from the one used in the design procedure where we assumed the input power was constant. To increase the accuracy of the model, it was necessary to include the influence of the arc characteristics in the model.

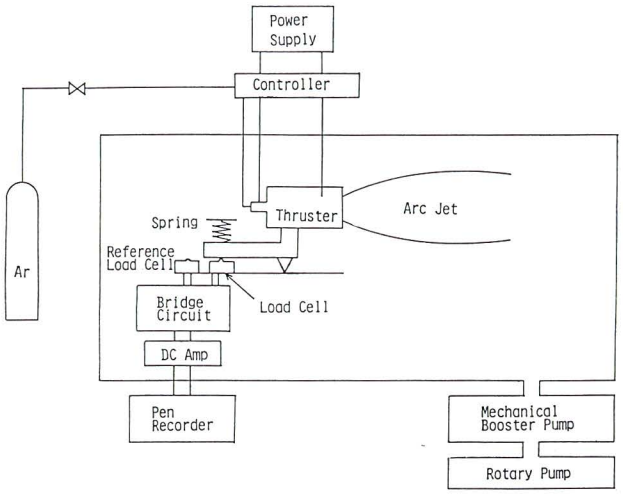

Fig. 6. Experimental Block Diagram.

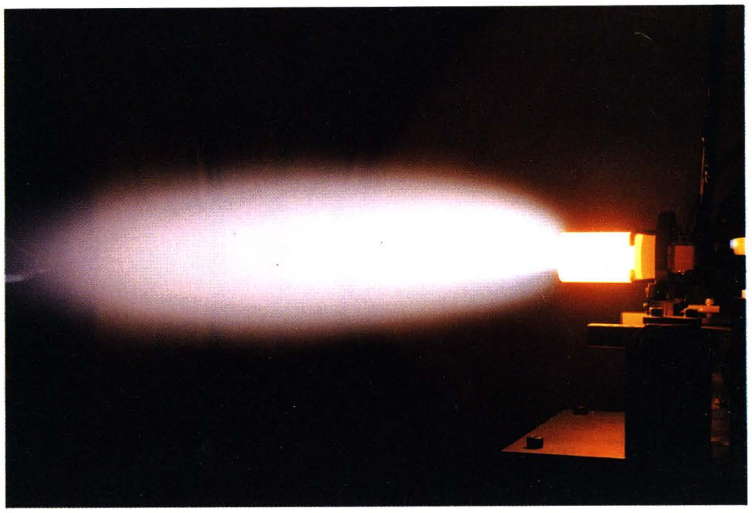

Fig. 7. Picture of the Thruster in Operation.

5. Results and Discussion

Figures 9(a) and 9(b) show the mass flow rate-thrust and the mass flow rate-specific impulse characteristics. The solid line denotes the calculated results from the model and the circle denotes the experimental results. In the calculation, the experimental input power was employed. The variations of the experimental and calculated thrusts and specific impulses for mass flow rates show satisfactory agree-

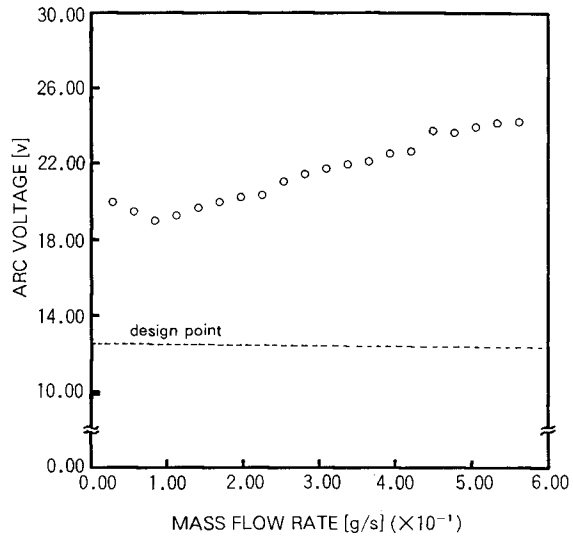

Fig. 8. Arc Characteristics.

ment. However, the results from the model are higher than the experimental ones. This is explained by the fact that the estimated η_p is larger than the actual one. In order to estimate an appropriate value for η_p, the thruster performance was calculated again with the input power obtained in the experiment. After making some calculations, 0.15 was found to be appropriate for η_p. The performance characteristics for this case are shown in Figs. 10(a) and 10(b). The calculated results coincide with the experimental results fairly well.

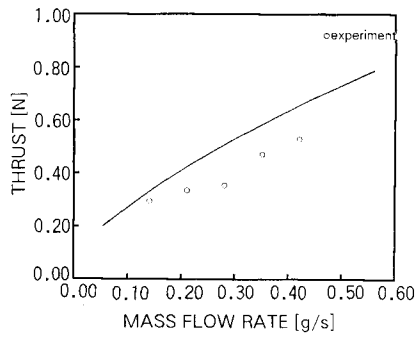

(a)

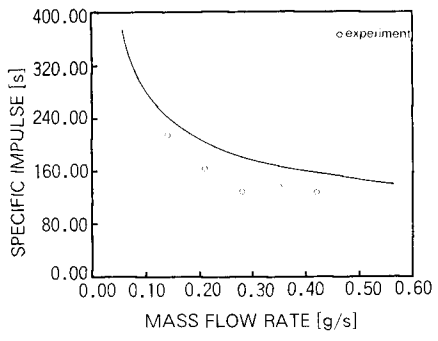

(b)

Fig. 9 (a) Mass Flow Rate—Thrust Characteristics (η_p=0.25).

Fig. 9 (b) Mass Flow Rate—Specific Impulse Characteristics (η_p=0.25).

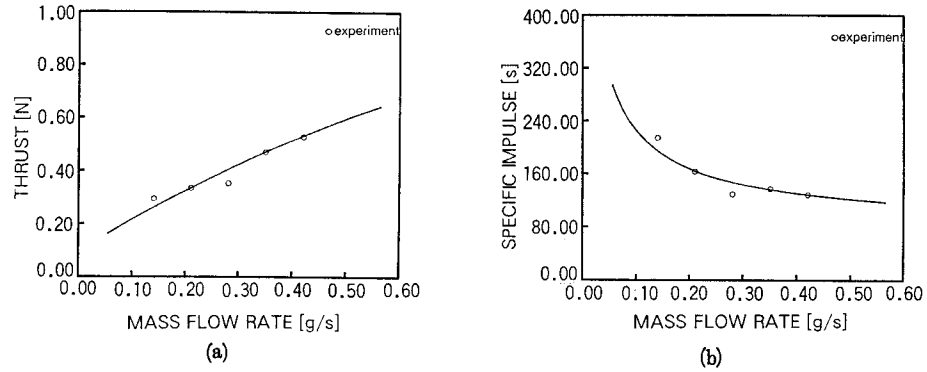

Fig. 10 (a) Mass Flow Rate—Thrust Characteristics (η_p=0.15).

Fig. 10 (b) Mass Flow Rate—Specific Impulse Characteristics (η_p=0.15).

6. Conclusion

A thruster model which can be used for the design of the arcjet thruster was proposed. The calculated performance characteristics were compared with the experimental ones. The following conclusions were drawn:

1) The influence of the design parameters on the thruster performance can be clearly understood from the present simplified quasi-one-dimensional model. The performance characteristics of the thruster are predictable from the flow model proposed here.

2) The value of 0.25 for the power conversion efficiency is overestimated. It is appropriate to set it at 0.15 for the low power DC arcjet thruster with a radiation cooling system.

References

1) Ao, T. and Fujiwara, T.: Numerical and Experimental Study of an MPD Thruster, In *Proceedings of the 17th International Electric Propulsion Conference*, Tokyo 1984, pp. 56–64.

2) Yamada, H. and Fujiwara, T.: Computational Fluid Dynamics Study of an MPD Thruster, *Memoirs of Faculty of Engineering, Nagoya University*, 38 (1986), pp. 261–278.